Preparation and characterization of amorphous multi-layers of Silicon Al and Ag

[1]H. El-Desouky, [1]S. Hassan, [2]A. El -Shaer, [1]M. S. Abo Ghazala, [3]T. Y. Elrasasi*

1Faculty of Science, Menofia University, Shebeen El-Koom, Egypt
2Faculty of Science, Kafrelshiekh University, Kafr Elshaikh, Egypt.
3Physics department, Faculty of Science. Benha Univesity, Benha, Egypt.

Thin layers composed of Si/Si, Si/Al, Si/Ag, and Si/Al/Ag were deposited on quartz substrate through the process of thermal evaporation, followed by a heat treatment at 500 °C for one hour. The characteristics related to the structure and light interaction of these films were thoroughly analyzed. X-ray diffraction (XRD) techniques showed a broad band around 2Θ =20-30 related to the amorphous silicon and some small peaks appeared after the heat annealing. EDX of the prepared multilayers showed that the samples were exposed to oxidation. Scanning electron microscope (SEM) showed the formation of polycrystalline phases of Si/Al, Si/Ag, and Si/Al/Ag which are distributed all over the film's surfaces. FT-IR measurements showed the characteristic peaks of Si, Al, and Ag. Optical absorption measurements indicated an increase in the absorption coefficient. Integration of (Si/Al/Ag) nanoparticles increased the absorption in the range of 400–1100 nm. The energy band gap of the prepared samples has been calculated (around 1.5 eV). The effect of oxidation on the activation energy has been studied by using the DC measurements.

Keywords
Amorphous Silicon, Surface Plasmon, Multilayers, Annealing
*: tarek.elrasasi@fsc.bu.edu.eg

Receive Date: 11 March 2024; Revise Date: 29 June 2024; Accept Date: 4 July 2024; Publish: 12 July 2024

Egypt J. Solids, Vol. (46) (2024)

1. Introduction

The technique of metal-induced crystallization (MIC) for transforming amorphous silicon and germanium into crystalline forms is gaining attention, particularly for its application in photo-detectors and solar panels. There's an interest in silicon MIC, prompting efforts towards innovative production strategies and technologies aimed at improving performance while reducing expenses [1]. Extensive research has been conducted on deploying silicon thin layers on economical bases like glass for optoelectronic devices and solar energy conversion systems [2,3]. Due to its advantage of low-temperature deposition and processing, amorphous silicon is frequently chosen for such uses. However, the relatively lower electron transport capability of amorphous silicon as opposed to its polycrystalline counterpart has sparked investigations into techniques for producing polycrystalline silicon on glass, including liquid-phase crystallization, chemical vapor deposition (CVD), and laser-induced crystallization [4 , 5, 6].

However, such methods require high processing temperatures, limiting their applicability to substrates that have low melting points or necessitating the use of protective layers to hinder the flow of heat from hotter areas to the substrate [7]. In contrast, amorphous silicon can undergo processing at temperatures as modest as 400 ºC, a feature not shared by many materials. This process can yield films that exhibit grain sizes nearing 100 nm and possess precisely managed surface orientations [8].

In our previous studies, the fabrication of thin films of aluminum/silicon (Al/Si) and aluminum/silicon/tin (Al/Si/Sn) [9] utilizing the method of thermal evaporation. The transformation of amorphous silicon (a:Si) into its crystalline form was detected upon annealing at 500 °C, employing

Egypt. J. Solids, Vol. (46) (2024)

methodologies like Raman spectroscopy, x-ray diffraction, and field emission scanning electron microscopy for observation. The aluminum-induced crystallization (AIC) technique is initiated by applying a layer of polycrystalline aluminum onto the surface of a substrate, which is then succeeded by the addition of an amorphous silicon layer atop it. Following this, the combined layers are subjected to annealing at temperatures beneath the eutectic point of aluminum and silicon, a process that allows the amorphous silicon to permeate through the grain boundaries of the aluminum film [10]. As the silicon grains expand, they exert an upward force on the aluminum, causing a significant shift in the arrangement of the aluminum and silicon films. Additionally, it has been observed that exposing the aluminum layer to the air, allowing it to develop a thin layer of aluminum oxide (AlOx) before depositing the amorphous silicon, results in films that exhibit a distinct alignment. This oxide layer is thought to be crucial in facilitating such orientation, acting as a nucleation point for the growth of the silicon grains [11].

In general, the desired properties for silver and aluminum multilayers used as metallization contacts are as follows: low specific resistivity, good thermal stability, high uniformity across the flat substrate, low particle contamination, good adherence to the substrate, and low manufacturing costs.

In this study, the technique of MIC of amorphous silicon, utilizing it as a method for the thermal deposition of various metals onto silicon films to achieve the direct bandgap construction of Si/Al, Si/Ag, and Si/Al/Ag prepared through the thermal vacuum evaporation method. The addition of

Egypt J. Solids, Vol. (46) (2024)

silver in multilayers with silicon and aluminum metal enhanced the results of the optical and electrical properties.

2. Experimental

2.1. Materials

For the creation of Si/Al/Ag multilayers, high-purity Ag and Al sheets (99.99% purity) supplied by Sigma-Aldrich for chemicals were utilized. The layers of Ag and Al were applied over a silicon base using the thermal evaporation method. This process was conducted with a triple wire tungsten boat in a vacuum environment of 2×10^{-5} mbar, utilizing an Edwards E306A coating apparatus.

As depicted in Figure (1), the deposition process for aluminum, silver, and silicon multilayers via thermal evaporation was carried out with electrical currents of 42 amperes for Al and Ag, and 20 amperes for Si, resulting in multilayers of varying thicknesses. The measurement of the layer thickness was accomplished with a quartz crystal monitor (MAXTEK INC TM-100), indicating thickness values of 40.5 nm for Si/Si, 100 nm for Si/Al, 75 nm for Si/Ag, and 108.5 nm for Ag/Si/Al. Subsequently, all the prepared films underwent an annealing process in a vacuum of 2×10^{-3} mbar at 500 °C for one hour.

Egypt J. Solids, Vol. (46) (2024)

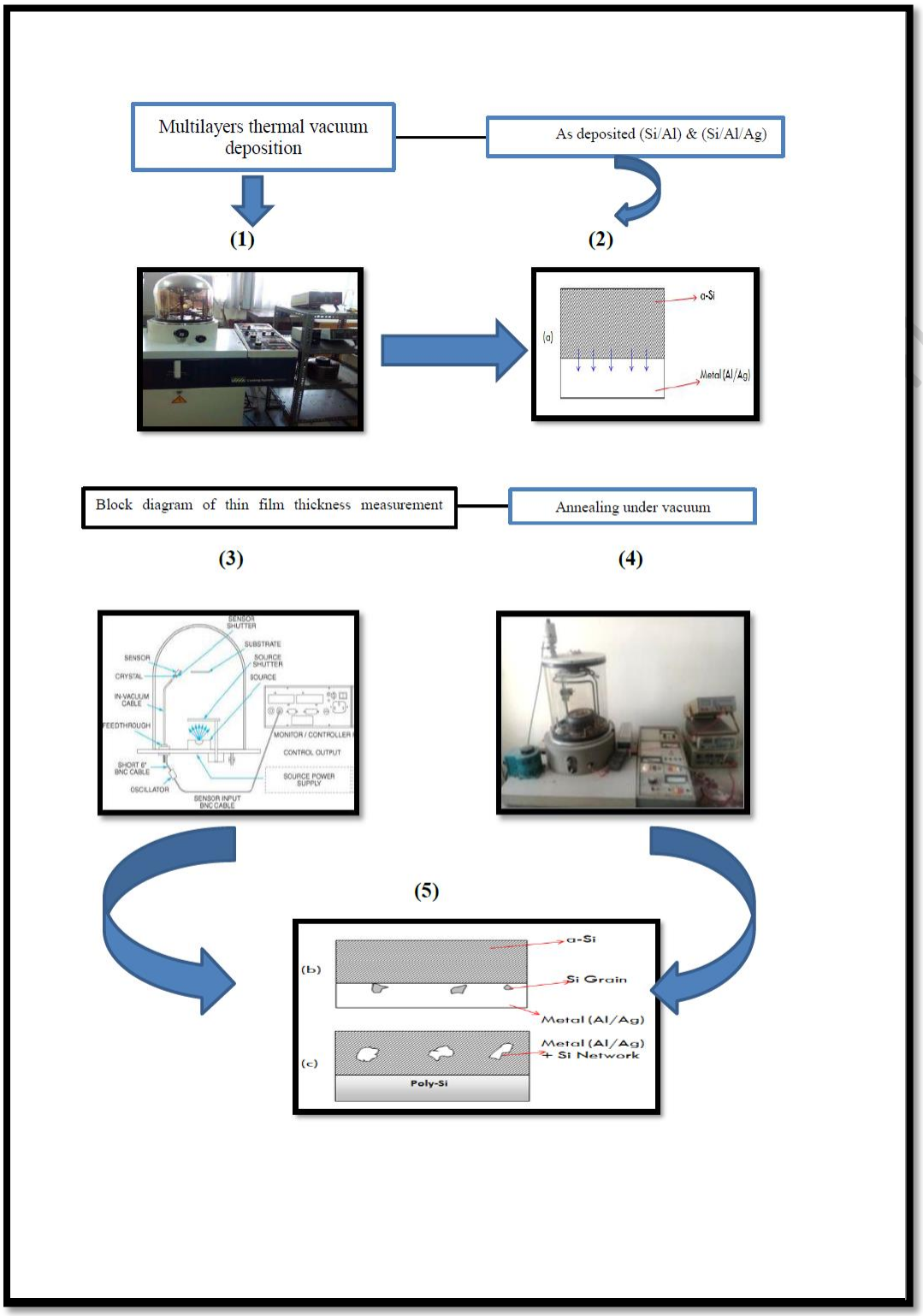

Figure (1) Illustrates the process and underlying mechanism for the creation of polycrystalline silicon multilayers utilizing a triple-wire boat within a thermal vacuum evaporation system.

2.2. Measurments

The prepared poly-crystalline silicon (Poly: Si) films have been examined using several techniques: x-ray diffraction (XRD) employing a SHIMADZU 6100 LabX system, scanning electron microscopy (SEM) with a QUANTA FEG 250 instrument, energy dispersive x-ray spectroscopy (EDX). To assess the optical characteristics of the films, a UV-VIS spectrophotometer (JASCO V-570) was utilized, covering a spectral range from 200 to 1100 nm. Furthermore, infrared spectra transmittance analysis was performed using a BRUKER VERTEX 80 spectrometer, the wavenumbers range is 400 to 4000 cm^{-1}.

3. Results

X-ray diffraction (XRD) was conducted on layers of Si/Si, Si/Al, Si/Ag, and Si/Al/Ag multilayers that were annealed at 500 °C for 1 hour to study the formation of poly-silicon prepared by MIC. The XRD analysis revealed a broad peak centered around a specific angle, typically ranging between $2\theta = 20°$ and 30°. In samples containing amorphous silicon, the XRD pattern did not exhibit clearly defined characteristic peaks. Instead, the broad peak indicated the presence of short-range order in the amorphous structure but lacked the long-range order necessary for sharp diffraction peaks found in crystalline materials. In contrast to crystalline silicon, which displays distinct diffraction peaks, amorphous silicon displayed a broad hump in its XRD pattern. The amorphous behavior results from the low time of annealing samples which is one hour, so some small peaks appeared in the range $2\theta = 40°$ indicating partially crystalline appeared in the annealed samples [12].

Egypt J. Solids, Vol. (46) (2024)

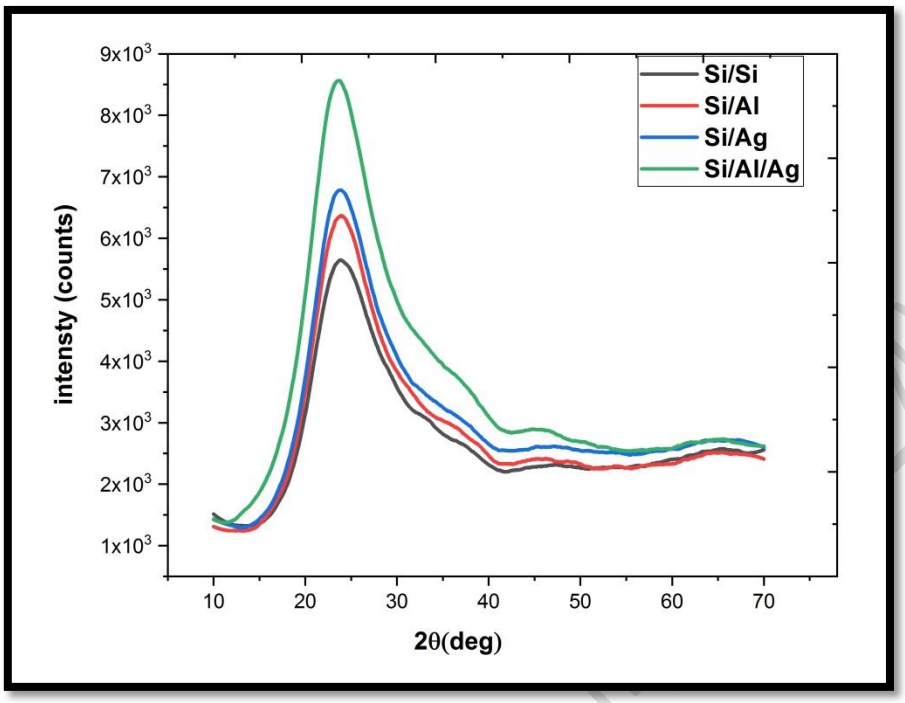

Figure (2) XRD patterns of the Si/Si, Si/Al, Si/Ag and Si/Al/Ag after annealing at 500 °C for one hour

Table 1. Lattice Parameters of Si/Si, Si/Al, Si/Ag and Si/Al/Ag multilayers

Sample	**h k l**	**2θ (degrees)**	**d-spacing (Å)**
Si/Si	1 0 1	21.4	4.3
Si/Al	2 0 0	22.9	3.87
Si/Ag	2 1 1	23.7	3.66
Si/Al/Ag	1 3 0	23.7	3.69

Figure (3) Illustrates the EDX pattern displays Si/Si, Si/Al, Si/Ag, and Si/Al/Ag films, with the Si content combined with the metal elements deposited on the quartz substrate sample. The information obtained from the EDX analysis is presented in Table 2, this is also evident of the rise in oxygen content, suggesting that the Si layer is undergoing oxidation, which results from partial vacation which allowed oxygen to penetrate the samples

Egypt J. Solids, Vol. (46) (2024)

causing an a eutectic phase transition of various SiO2 phases according to the following reaction Eq. (1)

$$\mathbf{Si + O_2 \longrightarrow SiO_2 \quad (1)}$$

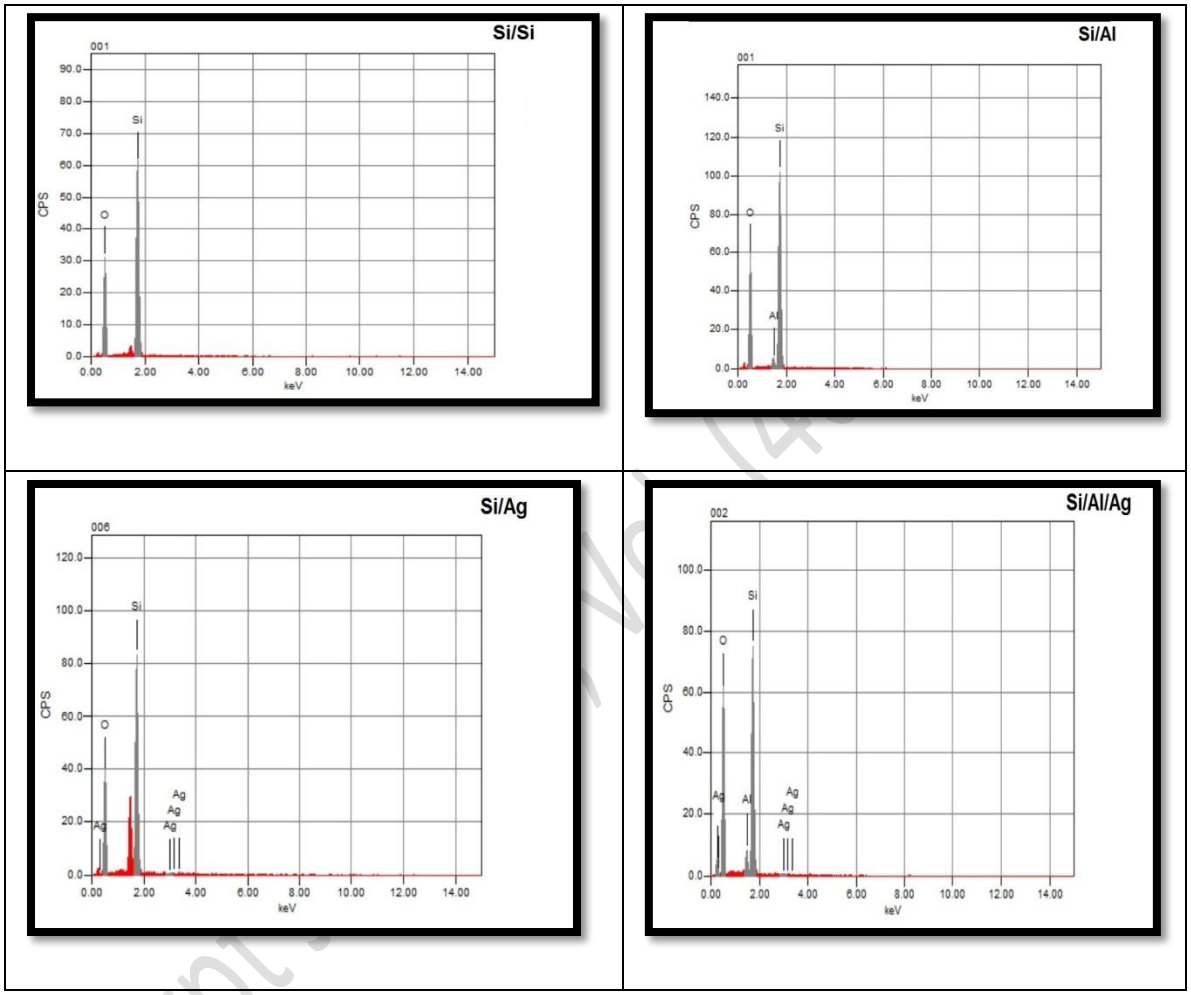

Figure (3) EDX pattern for Si./Si/Al, Si/Ag, and Si/Al/ Ag multilayers annealed at 500 ^{o}C

Table (2): elements percentages of Si/Si, Si/Al, Si/Ag, and Si/Al/Ag multilayers

	Element	Si/Si	Si/Al	Si/Ag	Si/Al/Ag
Weight %	**Si**	41.85	37.6	40.84	21.82
	Al	-	1.51	-	2.12
	Ag	-	-	0.22	0.32
	O	58.15	60.87	58.93	60.0
Atomic %	Si	29.07	25.76	28.29	26.28
	Al	------	1.07	-	8.27
	Ag	-----	----	0.04	0.03
	O	70.93	73.17	71.67	64.77
Particle size (nm)		100	100	100	100

Scanning Electron Microscopy (SEM).

Figure (4) shows the SEM analysis on amorphous silicon (a-Si) that was applied to a quartz base. The films of Si/Si, Si/Al, Si/Ag, and Si/Al/Ag underwent annealing at 500 ºC for one hour to assess their structural characteristics and interlayer interactions. Figure (4.a) displays a layer of amorphous silicon lacking discernible crystalline structures. Meanwhile, Figure (4.b) shows formations of crystallite clusters, signifying the emergence of polycrystalline silicon within the Si/Al films. This transformation in the amorphous silicon films is facilitated through a eutectic reaction during the process of aluminum-induced crystallization [13,14]. This reaction leads to the formation of crystallites that cluster

Egypt J. Solids, Vol. (46) (2024)

together, creating formations that resemble islands [15,16]. As more metallic elements are layered on, these islands increase in number, eventually merging to form a network of silicon islands. In the case of Si/Ag, the surface of the Si/Ag films can be seen in Figure (4.c), showing the initial stages of silver metal diffusion through silicon layers. The shape of the particles has become more globular and the gap between them has widened. This similar morphology was also observed in other experiments. [17].

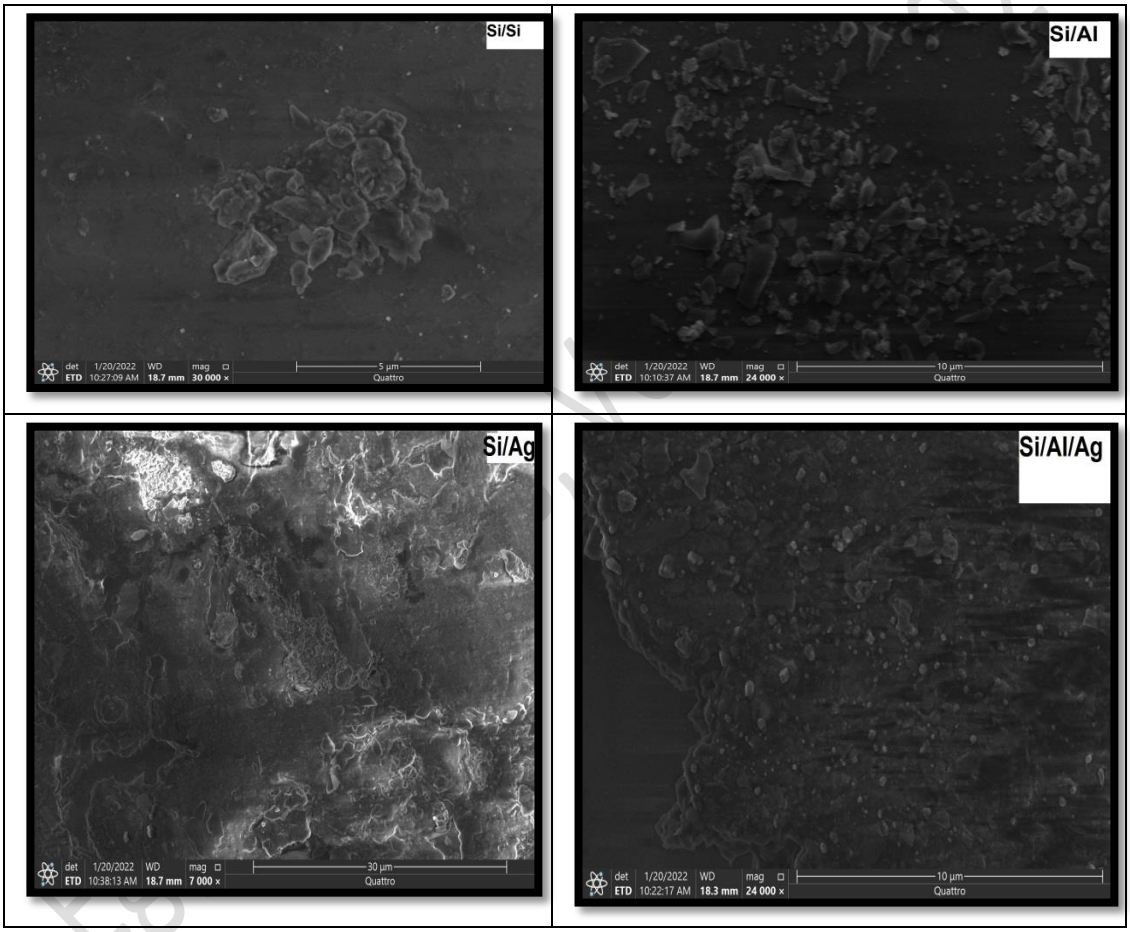

Figure (4): SEM micrograph of Si/Si, Si/Al, Si/Ag, and Si/Al/Ag multilayers annealed at 500 °C

Figure (4.d) depicts the structure of Si/Al/Ag multilayers, demonstrating that aluminum and silver induced crystallization in the layers,

leading to a decrease in grain boundaries as the area of these islands increases by improving electron mobility.

Scanning electron microscopy (SEM) images of Si/Al/Ag multilayers reveal brighter islands with Si/Ag thin film, which affected the formation of coatings, resulting in a more continuous and homogeneous distribution of materials in the films. The brightness of the islands is intensified by increased accumulation from the addition of the Ag top layer, which aids in surface texturing for light trapping and reducing light reflectance.

Figure (5) presents the FT-IR spectroscopy results for the layered configurations of Si/Si, Si/Al, Si/Ag, and Si/Al/Ag. The presence of (OH) groups was noted within the 3500–3800 cm^{-1} range. Absorption peaks observed around 472 cm^{-1}, along with faint bands near 393 and 400 cm^{-1}, are attributed to the stretching vibrations of Ag–O [18]. Furthermore, the spectral bands located near 1400 and 820 cm^{-1} are indicative of Si-O-Si linkages and Al-O bending motions, respectively. The details of all identified bonds are systematically listed in Table 3.

Egypt J. Solids, Vol. (46) (2024)

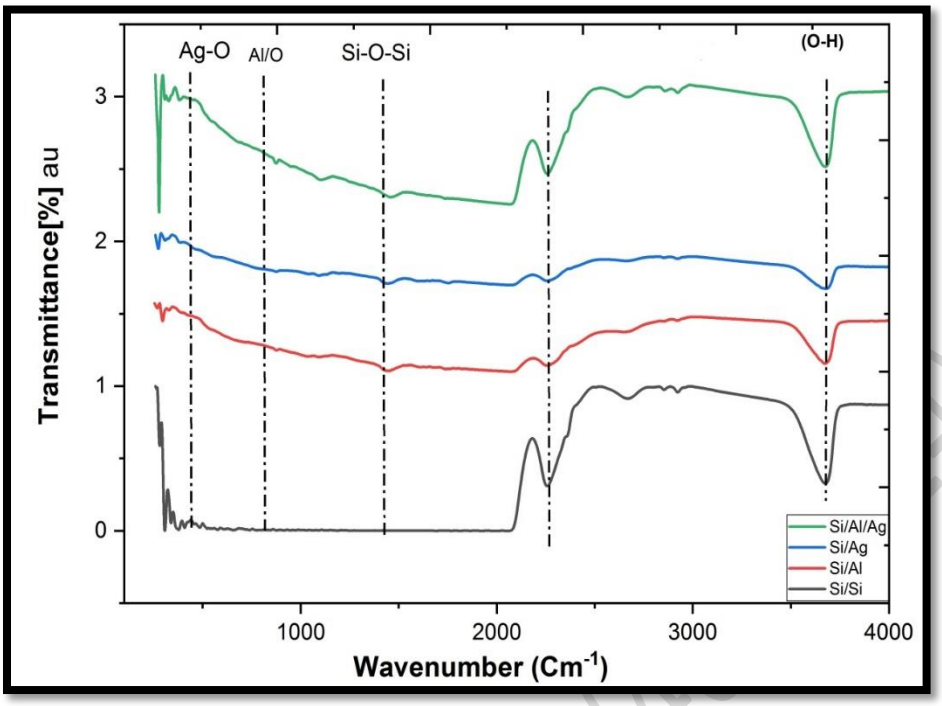

Figure (5): FTIR spectra for Si /Si, Si/Al, Si/Ag, and Si/Al/Ag multilayers annealed at 500 ºC.

Table (3): FT-IR spectra for Si /Si/Al, Si/Ag, and Si/Al/Ag multilayers annealed at 500 ºC.

Wave number cm^{-1}	Band assignment	Si	Si/Al	Si/Ag	Si/Al/Ag
3600	O-H group	3689	3660	3676	3676
2260		2247	2260	2253	2260
1400	Si-O-Si stretching	------	1432	1450	1468
820	Al-O stretch		820		874
1080	Al-O-Si		1065		1101
400	Ag–O			393	400

Figure (6) displays the UV-Visible absorption spectra for the multilayer structures of Si/Si, Si/Al, Si/Ag, and Si/Al/Ag. The absorption peaks showcased in parts (a), (b), (c), and (d) of Figure (6) occur at

Egypt J. Solids, Vol. (44) (1) (2024)

wavelengths of 557, 467, 459, and 365 nm, respectively. Notably, the peak at the shortest wavelength, approximately 365 nm, suggests a blue shift in the surface plasmon resonance (SPR) behavior of the aluminum and silver nanoparticles embedded in the silicon framework **.**

The shift towards higher energy levels in the absorption peak of the material's energy band gap is primarily influenced by the increase in carrier concentration due to Al-donor doping and the level of partially crystalline structure. The absorption coefficient (α) of the present sample can be determined by using the following equation Eq. (2):

$$\alpha = {}^{1243}/_{\lambda_x} \qquad (2)$$

where λx is the wavelength of the electronic transitions. These transitions are controlled by certain selection rules, which can be expressed by Eq. (3) and (4)

$$(\alpha h\upsilon) = A(h\upsilon - \mathrm{E}g)^n \qquad (3)$$

$$\mathrm{Log}\ (\alpha h\upsilon)) = \log \mathrm{A} + \ \mathrm{n} \log(\mathrm{h}\upsilon - E_g) \qquad (4)$$

where υ is the frequency, h is Planck's constant, A is a constant, E_g is the optical energy band gap and n is the power that characterizes the transition process. The n values show a direct transition to their values in the range of 0.5. The determination of direct optical energy gap by plotting the $(\alpha h\upsilon)^2$ vs. $h\upsilon$ as shown in Figure (7). The values of four samples are tabulated in Table (4). The calculated values of the samples are changed slowly from 1.42 to 1.6 eV. The alterations are because the band gap of doped a-Si changes based on the level of the dopant and whether the doping introduces new energy levels within the band gap . The band gap of the material could

Egypt J. Solids, Vol. (46) (2024)

potentially be increased or decreased based on the influence of doping on its electronic structure and the duration of annealing.

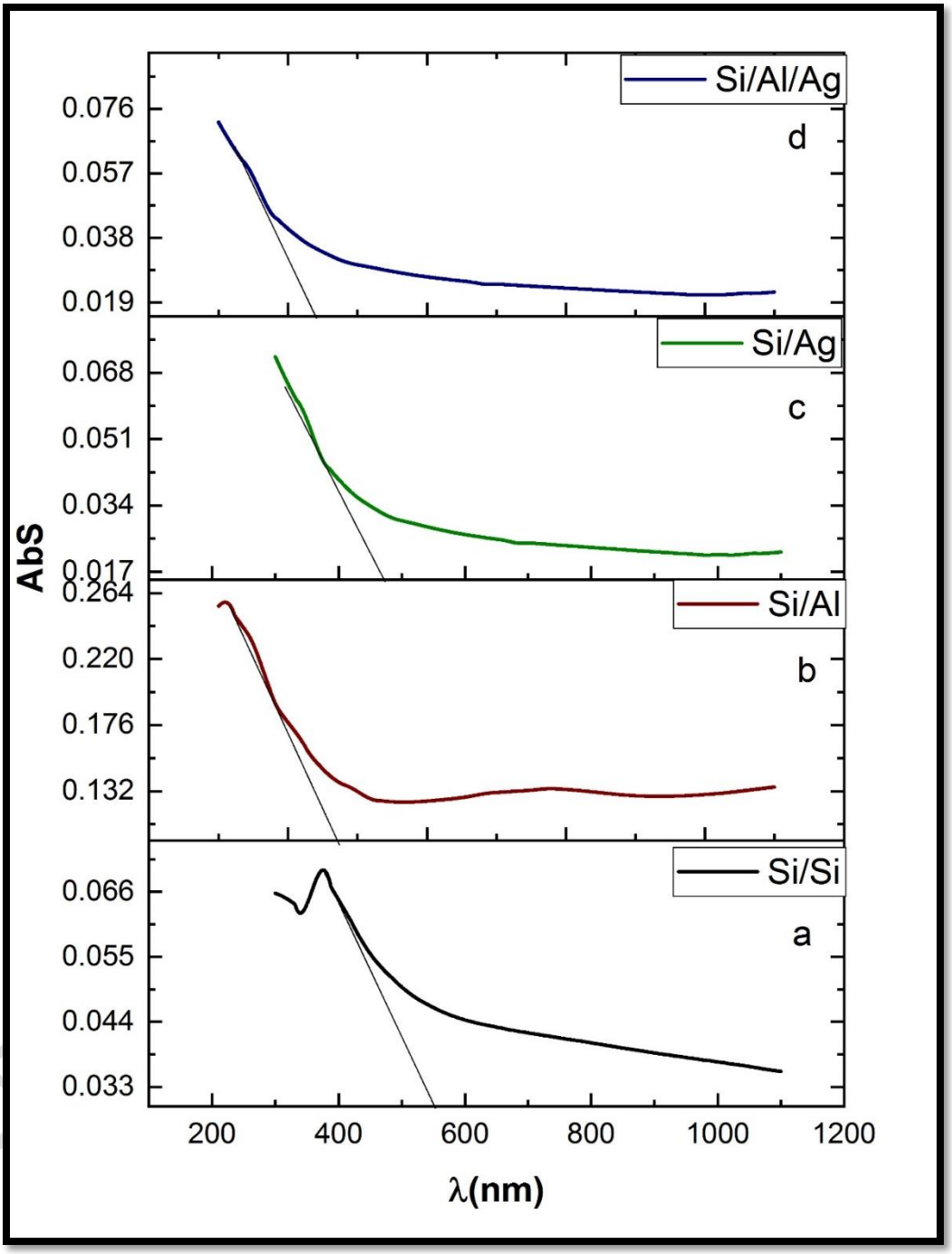

Figure (6) the optical absorption spectra of Si/Si, Si/Al, Si/Ag, and Si/Al/Ag

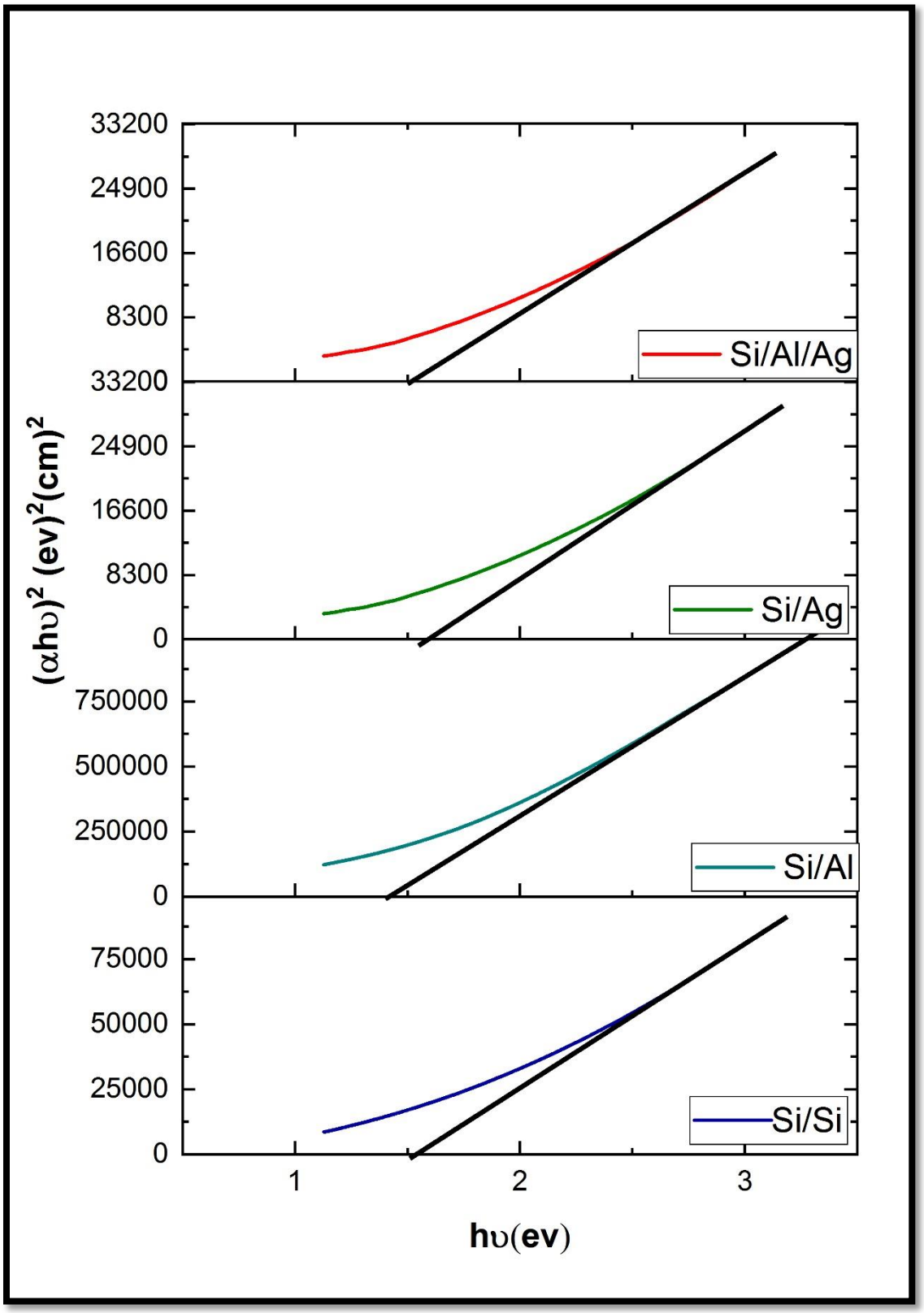

Figure (7) $\alpha h\upsilon^2$ vs $h\upsilon$ for Si/Si, Si/Al, Si/Ag, and Si/Al/Ag multilayers

Table (4): Energy band gap values for Si/Si, Si/Al, Si/Ag, and Si/Al/Ag multilayers.

Samples	Peak/position	E_g direct
Si/Si	374	1.5
Si/Al	312	31.4
Si/Ag	400	1.6
Si/Al/Ag	337	1.53

DC conductivity

Figure (8) illustrates the Ln(σ) against 1000/T $(K)^{-1}$, covering a temperature range from 303 to 373 K. From this graph, it is evident that the activation energy exhibits two distinct regions. The activation energy values were determined using the Arrhenius equation, denoted as equation (5), and these values are detailed in Table (5)

$$\sigma_{total} = A \exp(^{-E_a}/_{K_B} T) \qquad (5)$$

where A is the pre-exponential factor, E_a is the activation energy, and K_B is the Boltzmann constant. The values of E_a were determined through the least square fitting of equation (5). E_a for Si/Si is higher compared to Al/Si and Ag/Si samples. Silicon is recognized as a pure intrinsic semiconductor with a higher ionization energy than metals, which is almost equal to 0.85 eV . Additionally, there are variations in the conductivity levels of metals like Al and Ag based on temperature, suggesting a phase transition occurs in the structure within the temperature range measured for Si/Al, Si/Ag, and Si/Al/Ag samples. The energy levels within the energy gap of the partially

Egypt J. Solids, Vol. (46) (2024)

crystalline materials have decreased, leading to an increase in activation energy .

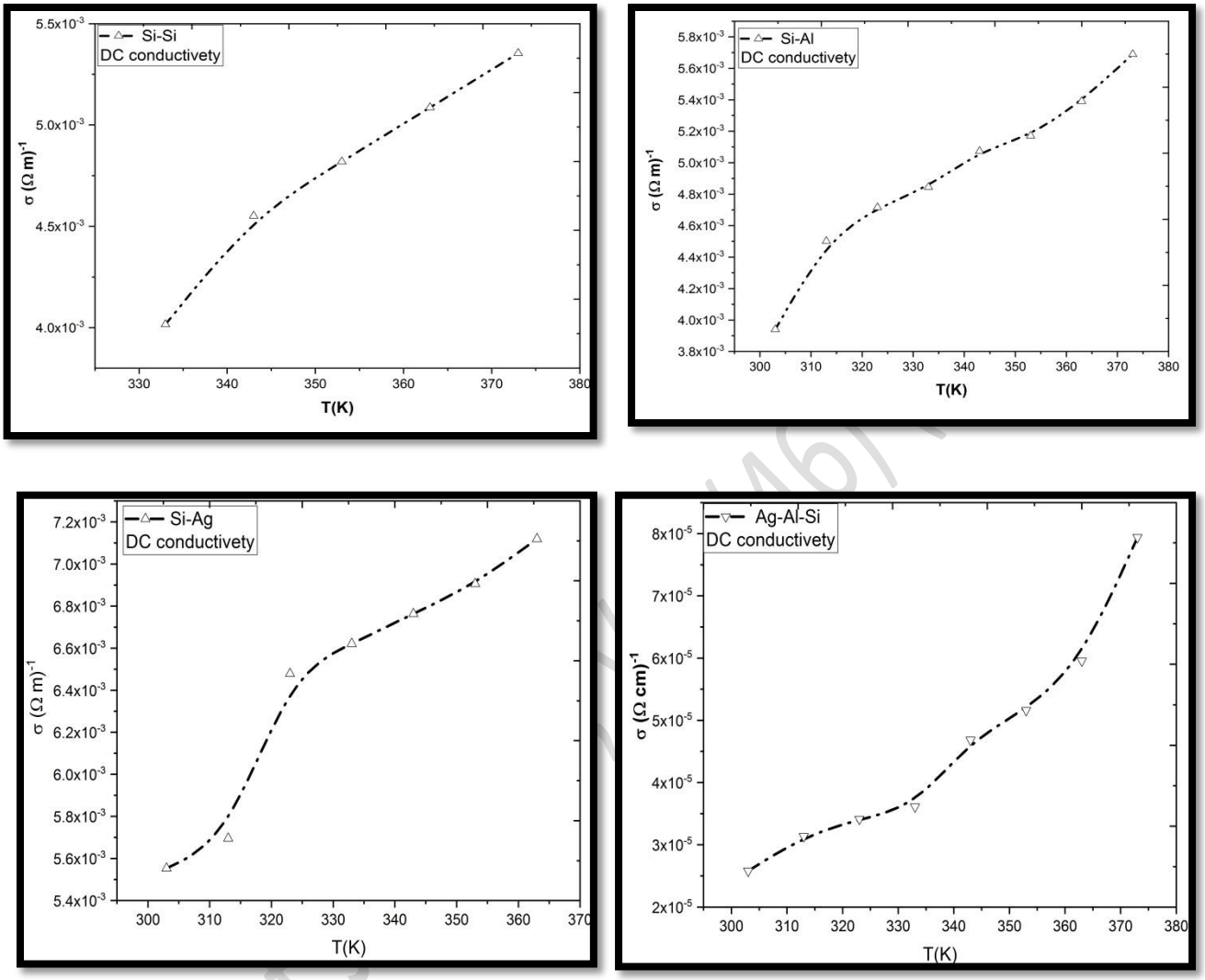

Figure (8) DC electrical conductivity of Si/Si, Si/Al, Si/Ag, and Si/Al/Ag multilayers as a function of the temperature

The Si/Al/Ag sample exhibits higher activation energy values based on observations this increase is likely attributed to enhanced oxidation in this specific sample. The oxidation process may introduce some defects like oxygen vacancies or interstitials into the material, these defects can serve as trapping sites for charge carriers, leading to an elevation in activation energy

for processes involving carrier transport or recombination. The formation of an oxide layer on the material's surface can act as a barrier that limits the diffusion of dopants or other species within the material, resulting in a rise in activation energy for diffusion-controlled processes. Furthermore, alterations in the electronic structure caused by oxidation, such as the creation of defect states or changes in the band gap, can affect the activation energy for electronic transitions and defect-related events affect the activation energy for electronic transitions and defect-related phenomena. The high level of oxidation can be seen in EDX .

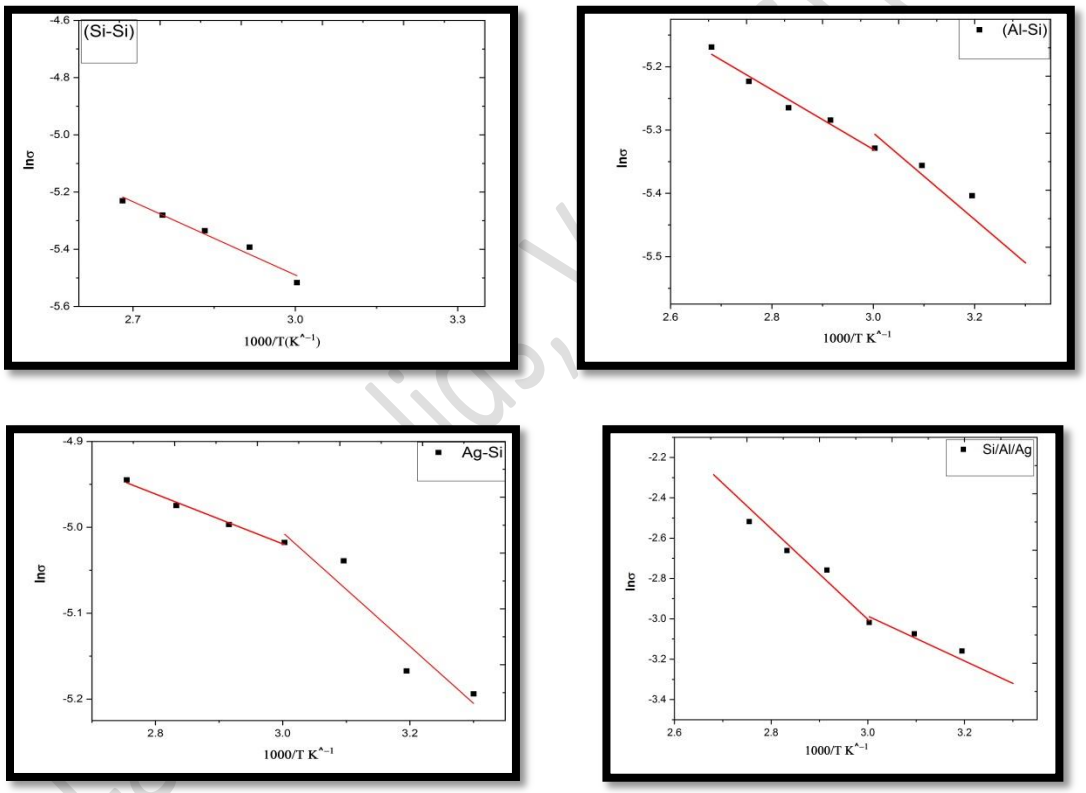

Figure (9) Ln (σ) V.S 1000/T (K)^$^{-1}$ plot for Si/Si, Si/Al, Si/Ag, and Si/Al/Ag

Table (5) Values of the activation energy of the Si/Al/Ag samples multilayers

Elements	**Si-Si**	**Al/Si**	**Ag-Si**	**Ag/Si/Al**
Activation energy (eV) Region 1	0.85163	0.4711	0.2898	1.49
Activation energy (eV) Region 2	--------	0.6883	0.662	0.73

Conclusion:

Amorphous silicon was synthesized through aluminum and silver-induced crystallization by employing a thermal evaporation method with a uniquely designed boat. A variety of multilayers, including Si/Si, Si/Al, Si/Ag, and Si/Ag/Al, were coated onto glass substrates at ambient temperature and subsequently annealed at 500 ºC for an hour. X-ray diffraction analysis revealed that all the samples exhibited amorphous characteristics, with broad peaks occurring between 20° and 30°. Evidence of significant oxidation in the samples was confirmed through energy-dispersive X-ray spectroscopy and scanning electron microscopy analyses. This oxidation notably influences the energy band gap, which was determined to be approximately 1.5 eV from UV-VIS spectroscopy measurements, as well as the activation energy derived from the DC conductivity assessments.

Egypt J. Solids, Vol. (46) (2024)

Declaration of Conflicting Interests

The author(s) declared no potential conflicts of interest concerning the research, authorship, and/or publication of this article.

References:

[1] M. S. Abo Ghazala, H. A. Othman, M. L. Sharaf El-Deen, M. A. Nawwar, and A. B. Kashyout**,** "Fabrication of Nanocrystalline Silicon Thin Films Utilized for Optoelectronic Devices Prepared by Thermal Vacuum Evaporation." ACS OMEGA. vol. 5, 42 (2020) 27633-27644.
DOI: 10.1021/acsomega.0c04206

[2] M. A. Nawwar, M. S .Abo Ghazala, L. M. Sharaf El-Deen, A. El-Shaer, B. Anis,A. B. Kashyout, "Toward White Light Random Lasing Emission Based on Strained Nano Polygermanium Doped with Tin via Metal-Induced Crystallization (MIC)" Cryst. Growth Des. vol. 23, 2, (2023) 751–768.
Doi.org/10.1021/acs.cgd.2c00970

[3] M. A. Nawwar, M. S. Abo Ghazala, L. M .Sharaf El-Deen, Kashyout. "Impact of strain engineering and Sn content on GeSn heterostructured nanomaterials for nanoelectronics and photonic devices" RSC Advances.. vol. 12, 38 (2022) 24518-24554.

Doi: 10.1039/d2ra04181b.

[4] S. D. Brotherton, "Polycrystalline silicon thin film transistors "Semiconductor Science and Technology, Vol 10 (1995)721

Doi.org/ 10.1088/0268-1242/10/6/001.

[5] A. Shah, P. Torres, R. Tscharner, N. Wyrsch, and H. Keppner, "Photovoltaic Technology: The Case for Thin-Film Solar Cells" Science Vol 285, 5428 (1999) 692–698.
Doi.org/10.1126/science.285.5428.692

[6] B. Rech, T. Repmann, M.N. Van den Donker, M. Berginski, T. Kilper, J. Hupkes, S. Calnan, H. Stiebig, and S. Wieder, "Challenges in microcrystalline silicon based solar cell technology" Thin Solid Films Vol 511 (2006) 548-555.
Doi.org/10.1016/j.tsf.2005.12.161

[7] G. Fortunato, A. Pecora, and L. Maiolo. Process, "Polysilicon thin-film transistors on polymer substrates" Mater. Sci. Semicond. Proce. Vol 15, 6 (2012) 627-641.

Doi.org/10.1016/j.mssp.2012.05.012

[8] O. Nast, T. Puzzer, L. M. Koschier, A. B. Sproul, and S. R. Wenham "Aluminum-induced crystallization of amorphous silicon on glass substrates above and below the eutectic temperature " J. Appl Phys. letters Vol 73, (1998) 3214-3216.

Doi.org/10.1063/1.122722

[9] M. A. Nawwar, M. S. Abo Ghazala, L. M. Sharaf El-Deen, B. A Kashyout, “Impact of strain engineering and Sn content on GeSn heterostructured nanomaterials for nanoelectronics and photonic devices” RSC Advances. Vol 12, 38 (2022) 24518−24554

Doi. org/10.1039/d2ra04181b.

Egypt J. Solids, Vol. (46) (2024)

[10] N. Oliver, and S. R. Wenham. "Elucidation of the layer exchange mechanism in the formation of polycrystalline silicon by aluminum-induced crystallization." *J. Appl. Phys.* Vol 88 (2000) 124-132.

Doi.org/10.1063/1.373632

[11] A. Sarikov, J. Schneider, J. Berghold, M. Muske. Ina Sieber, S. Gall, W. Fuhs "A kinetic simulation study of the mechanisms of aluminum induced layer exchange process " J. Appl. Phys. Vol 107 (2010) 114318.

Doi.org/10.1063/1.3431385

[12] W. Knaepen, C. Detavernier, R. L. Van Meirhaeghe , J. Jordan Sweet , C. Lavoie, " In-situ X-ray Diffraction study of Metal Induced Crystallization of amorphous silicon" Journal of Thin Solid Films . Vol 516 (2008) 4946–4952

Doi.org/10.1016/j.tsf.2007.09.037

[13] O. Nast; S. Brehme, S. Pritchard, A. G. Aberle, S. R. Wenham, “Aluminium-induced crystallisation of silicon on glass for thin-film solar cells” Sol. Energy Mater. Sol. Cells Vol 65, 1-4 (2001) 385−392.

Doi.org/10.1016/S0927-0248(00)00117-3

[14] S. Minomura. "Pressure effects on the local atomic structure" Semiconductors and Semimetals . Vol. 21 A (1984) 273−290.

Doi.org.10.1016/S0080-8784(08)63031-8

Egypt J. Solids, Vol. (46) (2024)

[15] F. A. Ferri, A. R. Zanatta, I. Chambouleyron. "Metal-induced nanocrystalline structures in Ni-containing amorphous silicon thin films" J. Appl. Phys Vol 100 (2006) 094311.

Doi.org/10.1063/1.2362877

[16] S. Hu, P. C. McIntyre, " Nucleation and growth kinetics during metal-induced layer exchange crystallization of Ge thin films at low temperatures". J. Appl. Phys. Vol 111 (2012) 044908.

Doi.org/10.1063/1.3682110

[17] R. Santbergen, T. L. Temple, R. Liang, A. H. M. Smets, R.A.C.M.M. Van Swaaij, M. Zeman. "Application of plasmonic silver island films in thin-film silicon solar cells" J. of optics. Vol 14 (2012) 024010.

Doi.org/10.1088/2040-8978/14/2/024010

[18] K. Kayed, B. Chiyah, "The Structural and Optical Properties of Silver Oxide Thin Films Synthesized by Thermal Evaporation of Silver with Subsequent Annealing" Aerosol Sci. Eng. Vol 4 (2020) 271–276. Doi.org/10.1007/s41810-020-00072-4

Egypt J. Solids, Vol. (46) (2024)